JGR Solid Earth

RESEARCH ARTICLE
10.1029/2019JB018340

Inferring Crustal Temperatures Beneath Italy From Joint Inversion of Receiver Functions and Surface Waves

G. Diaferia[1], F. Cammarano[1], N. Piana Agostinetti[2,3], C. Gao[4], V. Lekic[4], I. Molinari[5,6], and L. Boschi[7,8]

[1]Department of Geoscience, Università Roma Tre, Rome, Italy, [2]Department of Geodynamics and Sedimentology, Faculty of Earth Sciences, Geography and Astronomy, University of Wien, Vienna, Austria, [3]Istituto Nazionale di Geofisica e Vulcanologia, Rome, Italy, [4]Department of Geology, University of Maryland, College Park, MD, USA, [5]Istituto Nazionale di Geofisica e Vulcanologia, Bologna, Italy, [6]Institute of Geophysics, ETH Zurich, Zurich, Switzerland, [7]Department of Geosciences, University of Padua, Padua, Italy, [8]Sorbonne Universites, UPMC Univ Paris 06, CNRS, Institut des Sciences de la Terre Paris (iSTeP), Paris, France

Key Points:
- Transdimensional inversion of surface waves and receiver functions helps to constrain V_S and V_P/V_S ratios in the crust
- High V_P/V_S values in the middle and lower crust suggest the presence of filled-fluid cracks
- Jumps in V_P/V_S are associated with the quartz alpha-beta transition, enabling the estimation of geothermal gradients

Supporting Information:
- Supporting Information S1

Correspondence to:
G. Diaferia,
giovanni.diaferia@uniroma3.it

Citation:
Diaferia, G., Cammarano, F., Piana Agostinetti, N., Gao, C., Lekic, V., Molinari, I., & Boschi, L. (2019). Inferring crustal temperatures beneath Italy from joint inversion of receiver functions and surface waves. *Journal of Geophysical Research: Solid Earth*, *124*. https://doi.org/10.1029/2019JB018340

Received 11 JUL 2019
Accepted 24 JUL 2019
Accepted article online 31 JUL 2019

Abstract Temperature distribution at depth is of key importance for characterizing the crust, defining its mechanical behavior and deformation. Temperature can be retrieved by heat flow measurements in boreholes that are sparse, shallow, and have limited reliability, especially in active and recently active areas. Laboratory data and thermodynamic modeling demonstrate that temperature exerts a strong control on the seismic properties of rocks, supporting the hypothesis that seismic data can be used to constrain the crustal thermal structure. We use Rayleigh wave dispersion curves and receiver functions, jointly inverted with a transdimensional Monte Carlo Markov Chain algorithm, to retrieve the V_S and V_P/V_S within the crust in the Italian peninsula. The high values (>1.9) of V_P/V_S suggest the presence of filled-fluid cracks in the middle and lower crust. Intracrustal discontinuities associated with large values of V_P/V_S are interpreted as the $\alpha - \beta$ quartz transition and used to estimate geothermal gradients. These are in agreement with the temperatures inferred from shear wave velocities and exhibit a behavior consistent with the known tectonic and geodynamic setting of the Italian peninsula. We argue that such methods, based on seismological observables, provide a viable alternative to heat flow measurements for inferring crustal thermal structure.

1. Introduction

Unraveling the thermochemical structure of the crust is fundamental for understanding of its tectonic, magmatic, and geodynamical processes, both at local and global scales. Crustal rheological behavior holds direct implications for deformation between plates, the storage of mechanical stress, and, consequently, the overall seismicity. Moreover, the crust influences magmatic processes, controlling their spatial and temporal evolution, the chemical signature of magmas, their emplacement, and eruptive style.

Within the crust, the temperature distribution controls the depth of the brittle-to-ductile transition (BDT; Rutter, 1986), marking the change from elastic (related to earthquakes nucleation) to plastic behavior. On time scales larger than fault rupture, temperature is the key factor affecting the viscosity and flow of the lower, ductile portion of the crust, with direct implications for processes such as exhumation and delamination (Ranalli, 2000). Our understanding of the respective contribution of crust and mantle to isostatic adjustments (i.e., uplift and subsidence on regional scales) is informed by our knowledge of the thermal structure at depth (Lachenbruch & Morgan, 1990). However, temperature is also a function of heat production of radiogenic isotopes, is related to the upwelling (or percolation) of fluids through fault systems, is affected by the heat flux from the mantle and by the accumulation of partial melts within the crust. The discrimination of the different contributions is rather challenging (for a more detailed discussion see Lachenbruch, 1970). Despite its importance, temperature is only poorly known at depth and it is commonly inferred via heat flow measurements in boreholes, assuming a purely conductive heat transfer mechanism. However, heat flow data are scarce, have poor spatial representativeness, and suffer from systematic errors due to the measurement technique employed in the borehole (Stein, 1995). Particularly in active regions, the assumption of a purely conductive heat transfer does not hold due to the prominent role of fluid upwelling (*advection*), as suggested by the typically high values of heat flow in these areas.

To overcome the limitations of heat flow measurements, a more accurate and spatially representative method is desirable. In this regard, an approach based on seismic velocities can provide better coverage and

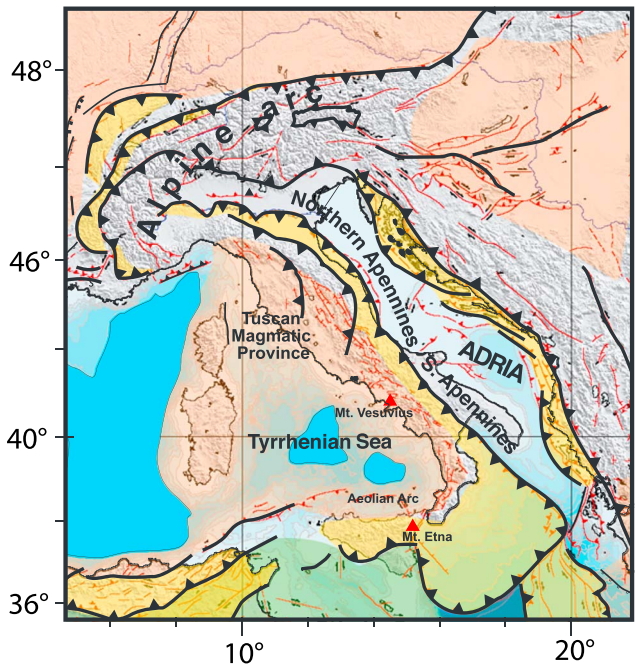

Figure 1. The tectonic setting of the Italian peninsula, modified from Faccenna et al. (2014).

less uncertainty. An attempt in this direction is made by Schutt et al. (2018) who used travel time anomalies of *Pn* waves for the retrieval of temperature at the Moho in western Unites States. In our work, we integrate two types of seismological data and infer the temperatures at depth by two independent methods: (i) detecting the seismic evidence of the temperature-driven transition of the quartz from the α to β form and (ii) using thermodynamics for translating seismic velocities into temperature. Specifically, we jointly invert dispersion curves of Rayleigh surface waves (SWD; from Molinari et al., 2015) and *Ps* receiver functions (RFs) using a reversible-jump Markov Chain Monte Carlo (rj-MCMC). The inversion method does not require strong prior information on the geometry of the subsurface structure and treats the number of model parameters as an unknown. The Bayesian nature of the inversion also enables the estimation of uncertainties of the model parameters.

The target of our study is the Italian peninsula (Figure 1), an area of recent tectonic activity and associated seismic and magmatic activities that are fundamental for understanding the broader contest of the central western Mediterranean. The Italian peninsula formed as a result of the Alpine and Apennine orogenic events, involving the African and European plates since the Cretaceous. In the past 15 Ma, the Appenine thrust rotated counterclockwise, causing the opening of the Tyrrhenian Sea basin. From the Eocene-Oligocene until the present, relevant volcanomagmatic activity occurred in several areas, such as the Tyrrhenian Sea basin, Aeolian Arc, Tuscany region, and the Neapolitan area, all of which are currently characterized by high heat flow measured at surface. A wealth of studies have been carried out to define the subsurface properties and structure, including those based on seismic reflection and refraction (Brückl et al., 2007; Waldhauser et al., 1998), *P* wave travel time tomography (Gualtieri et al., 2014; Serretti & Morelli, 2011), and high-resolution studies based on local earthquake arrivals (Diehl et al., 2009; Di Stefano et al., 2009). Crustal structure across the Apennines orogen has been also investigated through RFs (e.g., Piana Agostinetti et al., 2008). An integration of different seismological methods is attempted in Piana Agostinetti and Faccenna (2018) to define the depth and geometry of the Moho. The CROP project (Finetti, 2005) shed light on intracrustal features through deep seismic reflection. While these studies have mainly characterized the crust in terms of compressional-wave velocities, Verbeke et al. (2012), Molinari et al. (2015), and Kästle et al. (2018) used ambient noise to obtain the shear velocity distribution at depth. Despite the abundance of data, interpretation is made difficult by uneven coverage, varying resolution, and sensitivity of each method.

2. Data and Method

Among the wealth of seismic data available for the Italian peninsula, we rely on the database of Rayleigh phase velocities used in Molinari et al. (2015). These are retrieved from ambient noise (more details in the following section) and posses near-ideal coverage across the Italian peninsula as well as sensitivity to crustal depths. To recover the V_P/V_S at depth and increase the resolution of the ambient noise data, we integrate that database with RFs. In fact, RFs provide information on potentially sharp seismic discontinuities at depth. Isotropic, one-dimensional velocity profiles are obtained by joint inversion of the two data sets, using a rj-MCMC that does not require any prior discretization of the subsurface model. The number of layers is an unknown itself and, theoretically, is only constrained by the data when the prior information do not provide any restriction (Bodin & Sambridge, 2009; Gao & Lekic, 2018). The estimates of shear velocity and V_P/V_S ratio at depth are obtained as a posterior probability density function, indicating both their robustness and uncertainty. Finally, we use the information on shear waves velocity and V_P/V_S ratio both for detecting the quartz transformation to be used as a geothermometer and for estimating absolute temperatures through thermodynamics.

2.1. RFs

Teleseismic RFs from a number of permanent and temporary seismic networks have been collected to create a homogeneous database covering peninsular Italy (Piana Agostinetti et al., 2008; Di Bona et al., 2008;

Piana Agostinetti, 2015; Piana Agostinetti & Amato, 2009; Steckler et al., 2008). We only considered stations with more than two years of continuous raw-data availability, to ensure good back azimuthal coverage. To emphasize the high-frequency around 1 Hz, a Gaussian filter is used with parameter $a = 2$ (the higher the value, the larger the width of the filter and the frequency content of the output; Ligorria & Ammon, 1999). Following Bianchi et al. (2010), we extracted back azimuthal harmonic from each data set and obtained a single RF (the first angular harmonics, $k = 0$) that represents the 1-D, horizontally layered, isotropic structure beneath the seismic section (Park & Levin, 2016a). The uncertainty on each $k = 0$ harmonics is estimated by bootstrap resampling (Efron & Tibshirani, 1991; Licciardi et al., 2014), while data correlation along each RF is obtained by deconvolution of the vertical component with itself (Piana Agostinetti & Malinverno, 2010). The uncertainty on $k = 0$ harmonics and correlation function are then used to build the covariance matrix that allows the computation of the likelihood between data and model predictions during inversion (Piana Agostinetti & Malinverno, 2018). The forward solver used in the inversion routine is based on the Thomson-Haskell propagator matrix (Haskell, 1953; Thomson, 1950) for isotropic and horizontally layered media.

2.2. Dispersion Curves

The dispersion curves of Rayleigh phase velocities are computed by Molinari et al. (2015) from the passive, 1-year-long recordings (2008) of Verbeke et al. (2012) that cover the Alpine area as well as the majority of the Italian peninsula. Phase velocities are given on an evenly spaced 0.25° × 0.25° grid, for a period range of 5–45 s that is ideal for crustal imaging. At the locations where RFs are available, we interpolate the phase velocities at each frequency to obtain the dispersion curves to be used in the joint inversion. When dispersion curves were extracted from ambient noise recordings, the uncertainty on phase velocities was not evaluated. In this study, we assign an uncertainty of 0.03 km/s (~1%) to the SWD curves. It is worth noting that this value is rather conservative given the precision of the ambient noise method with even station coverage and recordings that are long in duration. Moreover, we assume that noise is uncorrelated across all frequencies/periods (i.e., a diagonal covariance matrix of the errors for SWD data; see below).

2.3. The Joint Inversion Strategy

2.3.1. The rj-MCMC Algorithm

We employ the approach presented in Bodin et al. (2012) based on a rj-MCMC scheme for the joint inversion of RF and SWD curves. The inversion problem is formulated with a Bayesian framework, where the final solution is represented by a posterior probability density function and is sampled through a transdimensional approach (Malinverno, 2002), that is, the number of model unknowns (e.g., the number of layers) is itself unknown. This approach avoids the requirement of any subjective a priori discretization of the solution (Piana Agostinetti & Malinverno, 2010). The rationale behind the method is to sample the posterior density function, combining our a priori knowledge of the subsurface and updating it with the information provided by the data. Formally, this is expressed by Bayes' theorem (Bayes & Price, 1763):

$$p(\mathbf{m}|\mathbf{d}_{\text{obs}}) \propto p(\mathbf{d}_{\text{obs}}|\mathbf{m}) \times p(\mathbf{m}) \tag{1}$$

where $p(\mathbf{m}|\mathbf{d}_{\text{obs}})$ is the posterior density function (expressed as the probability of having the model parameters in $\mathbf{m}$, given the observed data); $p(\mathbf{d}_{\text{obs}}|\mathbf{m})$ is the likelihood (the probability of observing the data, given the model); $p(\mathbf{m})$ is the prior, the information we have about the model in terms of probabilities, before observing the data. The likelihood is expressed as

$$p(\mathbf{d}_{\text{obs}}|\mathbf{m}) = \frac{1}{\sqrt{|\mathbf{C}|(2\pi)^n}} \exp\left\{\frac{-\phi(\mathbf{m})}{2}\right\}. \tag{2}$$

$\mathbf{C}$ is the covariance matrix of the data vector (since the error in a RF is strongly correlated; Di Bona, 1998) and $\phi(\mathbf{m})$ is the misfit between the vector of observed data $\mathbf{d}_{\text{obs}}$ and forward estimation $g(\mathbf{m})$ from the model, expressed as the Mahalanobis distance (Mahalanobis, 1936):

$$\phi(\mathbf{m}) = (g(\mathbf{m}) - \mathbf{d}_{\text{obs}})^T \mathbf{C}^{-1} (g(\mathbf{m}) - \mathbf{d}_{\text{obs}}) \tag{3}$$

The posterior density $p(\mathbf{m}|\mathbf{d}_{\text{obs}})$ cannot be directly computed; hence, it is sampled iteratively. At each step, the model is randomly perturbed (the Monte Carlo approach) to generate a candidate model that can be accepted or rejected. Thus, the resulting chain of models (the Markov Chain), if sufficiently long, will provide

Table 1
Prior Density Distribution and Standard Deviation of the Perturbation Allowed in Each Iteration of the rj-MCMC Inversion Algorithm

Parameter	Prior (uniform probability)	Perturbation (st. dev.)
V_S (km/s)	1.5–4.7	0.12
V_P/V_S	1.6–2.1	0.10
Density (g/cm^3)	2.4–3.1	3
Layer depth (km)	0–75	0.6

Note. rj-MCMC = reversible-jump Markov Chain Monte Carlo.

a reliable estimation of the posterior density. The Metropolis-Hasting criterion (Hastings, 1970; Metropolis et al., 1953) is used to decide on the retention of a candidate model for the *i*th iteration, favoring the proposed model if it leads to a decrease of the misfit with the observed data.

The perturbation of the current model occurs by randomly choosing among four options: change the velocity of a layer, change the thickness of a layer, add a layer and propose its velocity, and remove a layer. For every option, the new velocity (and/or layer depth) is drawn from a Gaussian distribution centered on the current value of each parameter. In Table 1 we show the prior, uniform, probability function of each variable we invert for, together with the perturbation allowed (in terms of standard deviation) for generating the candidate models along the chain. The possibility that the number of layers can indeed vary along the chain embodies the transdimensionality of the inversion algorithm. Despite the fact that we invert our data set for density, we do not consider it for further interpretation, due to the low sensitivity of both RFs and SWD to that parameter.

With respect to Bodin et al. (2012), we employ the rj-MCMC algorithm strategy with some modifications, motivated by our specific needs and observations. Bodin et al. (2012) keep the ratio V_P/V_S fixed in order to decrease the computational cost of the inversion. Following Piana Agostinetti & Malinverno (2010, 2018) and Gao and Lekic (2018), we decide to treat V_P/V_S as a variable that can be randomly perturbed along the chain. As a matter of fact, both laboratory experiments (Peng & Redfern, 2013; Ohno et al., 2006) and thermodynamic modeling (Diaferia & Cammarano, 2017) suggest that V_P/V_S can strongly vary at crustal depths as a result of the phase transition of quartz from its α to β form. Therefore, given the scope of this study, we find that fixing V_P/V_S at an arbitrary value will hamper an unbiased interpretation. Moreover, the algorithm in Bodin et al. (2012) is hierarchical, meaning that data error of both RFs and dispersion curves is itself an unknown that is estimated by inversion. However, this is not the case for our algorithm, which allows us to decrease the computational demand. Instead, we rely on the estimates of data variance of RFs and dispersion curves.

Additionally, we modify the approach proposed in Bodin et al. (2012) so that models that are implausible are rejected before computing their forward response. Criteria for rejection are (i) top layer denser and/or faster than deepest layer, (ii) V_P >8.5 km/s, and (iii) V_S >5 km/s. Thus, only models that are geologically meaningful are actually compared against the data, speeding up the convergence of the inversion and with no significant or undesired effects on the prior. Through dedicated tests, we find the optimal values for the perturbation of model parameters, in order to maximize the algorithm's efficiency of convergence (see Table 1). Smaller perturbations would require many iterations for convergence, whereas large perturbations inhibit the convergence itself (the algorithm would not be able to fully explore the regions with high likelihood). The amplitude of perturbation of model parameters along the chain results in an overall model acceptance rate around 33%. For each location, we run 10 independent chains, with 500,000 iterations each, on the DT2 supercomputer at the University of Maryland. For the first 90,000 iterations, models are not saved for the posterior (”burn-in phase”). Along the remaining iterations, the misfit stabilizes at a sufficiently low plateau, implying that the high likelihood region of the model space is reached. We assess convergence by comparing ensemble characteristics across more (30) and longer (1,500,000 iterations) chains, validating that their properties do not differ from those obtained using settings detailed above. Adding more and longer chains does not result in a significant gain in terms of sampling of the posterior density.

2.4. Thermodynamics

We use thermodynamic modeling to predict absolute temperatures at depth from seismic velocities. We employ the code `Perple_X` (Connolly, 2009), an algorithm that is based on Gibbs free energy minimization for the calculation of (i) the stable mineral association at any P-T, given a certain chemical composition and (ii) the density and seismic velocities of the resulting mineralogical aggregate. For our specific application to a crustal domain, we implement in `Perple_X` the thermodynamic database from Holland and Powell (1998), which accounts for the experimentally constrained shear moduli of Hacker and Abers (2004) and the data from Ohno et al. (2006) regarding the peculiar behavior of quartz at the α to β transition (T$\sim$ 580 °C). We assume the crustal composition of Rudnick and Gao (2003), parametrized into the upper, middle, and lower continental crust. To this composition, we introduce 1% of H_2O, thus allowing the modeling of hydrated minerals (e.g., amphibole) and the formation of melt for a more realistic representation of the actual crust at high temperature. The assessment of the main parameters, that is, water and composition in addition to temperature and pressure, has been carried out by Guerri et al. (2015) and Diaferia and Cammarano (2017).

We correct the observed V_S to account for porosity. In doing this, we increase the seismically inferred velocities to the values expected for rock that is a pore-free mineralogical aggregate, which is the underlying approximation in thermodynamic modeling. Porosity as a function of depth is estimated with the empirical, quadratic formula in Vitovtova et al. (2014):

$$log\phi = -0.65 - 0.16h + 0.0019h^2 \tag{4}$$

where ϕ is the porosity (%)and h the depth in kilometers. Porosity at depth is then used to correct the observed shear wave velocities using the empirical relation $V_{\mathrm{Scorr}} = V_S + 7.07\phi$ in Castagna et al. (1985). After such correction, the observed velocities can be fitted to those modeled through thermodynamics and the corresponding temperature estimated.

3. Results

To estimate the crustal temperature from our seismic observations, we need to accurately characterize the shear wave velocities and V_P/V_S ratio of the subsurface. Therefore, it is important to first analyze the performance of the Bayesian inversion in fitting the observed data. The misfit between observed data and forward response of the inverted model is not homogeneous across locations. In several cases, it is rather difficult to retrieve a subsurface model that reconciles both RFs and surface wave dispersion. In the discussion, we provide a possible explanation for these observations. A comparison between observed and inverted data for all the 50 stations are given in the supporting information (Figure S1). Inversion results at these stations are also given in the supporting information (Figure S2), together with the corresponding model from Molinari et al. (2015) as a comparison.

In order to evaluate the fits to different data sets, we plot the misfit of the mean inverted model with the observed RFs and SWD at each station, normalized to the highest misfit recorded. Results are shown in Figure 2. The fit to the RFs (Figure 2, left panel) is particularly good in the southeastern part of the peninsula (e.g., MRVN station in the supporting information) and in specific locations of the Adriatic and Tyrrhenian sides of the Apennines. In the rest of the Peninsula, the RFs are very complex and more difficult to fit. The SWD data misfit is generally very low for all stations. However, it can be seen that stations in the Northern Apennines have the worst fit, especially at longer periods. Interestingly, this is the area where also the RFs fit is rather poor. Tork Qashqai et al. (2018) have pointed out similar difficulties in jointly fitting dispersion curves and RFs for certain locations in the central western United States where major structural complexities are expected.

Based on data misfit and visual inspection of results, we select 19 stations that are most reliable for the interpretation phase. Considering the mean V_S profile of the ensemble solution at all 19 stations, V_S shows a clear bimodal distribution with distinct peaks at 3.3 and 4.3 km/s (see Figure 3, left panel), reflecting the sensitivity of the data to both crustal and upper mantle depths. The V_P/V_S ratios show a more unimodal pattern with a peak at 1.76 (Figure 3, right panel), though higher values between 1.85 and 1.95 are also frequently found.

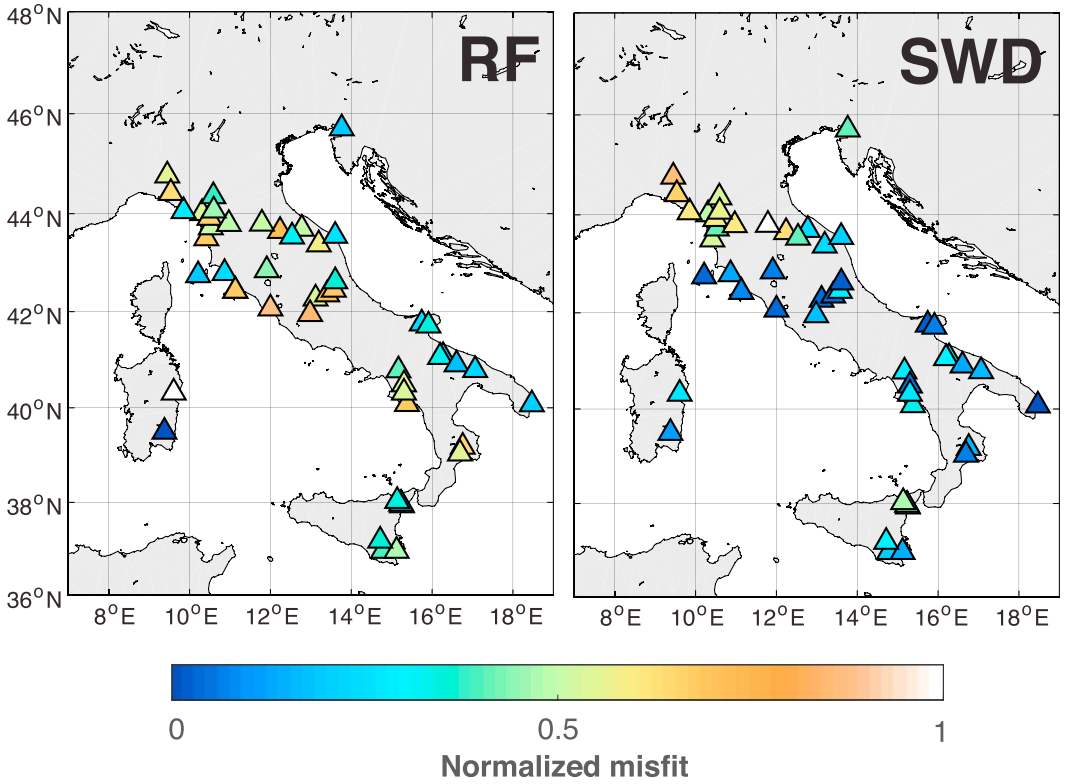

Figure 2. Misfit between the prediction of the mean model after inversion, for receiver functions (left) and surface waves dispersion curves (right). The misfits are normalized so that the maximum is unity. The RFs in the central and northern part of the Apennines are systematically more difficult to fit than in the rest of the peninsula. Here, the dispersion curve misfit is also higher (especially at longer periods), though generally good for the whole data set. Considering the combined misfit of both RF and SWD, we focus on 19 stations with best data fits. RF = receiver function; SWD = Rayleigh surface wave.

An example of the inversion outcome is shown in Figure 4 for the station AOI, situated in the Adriatic side of the Apennines. The panels on the left-hand side and in the center represent the posterior probabilities for V_S and V_P/V_S, respectively. The solid line indicates the mean model of the ensemble solution and the dashed line is its uncertainty in units of σ. On the right, the panel shows p(discontinuity), the posterior probability of having an interface. The V_S structure is rather homogeneous in the first 19 km, probably reflecting the low sensitivity of ambient noise in imaging small velocity changes in such depth range, rather than an actual

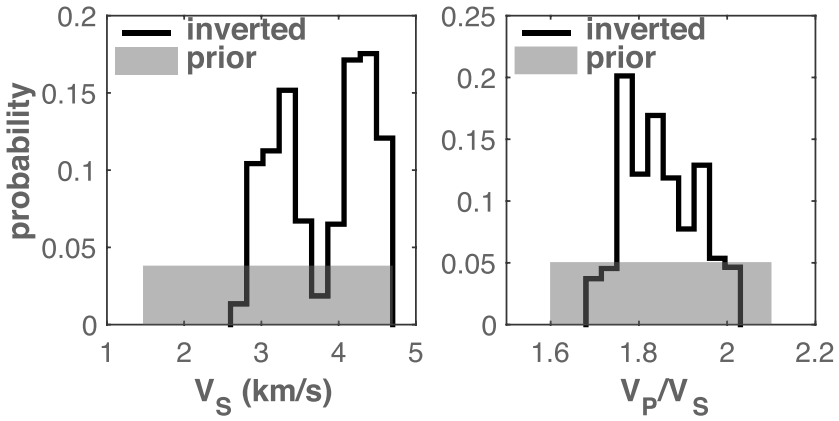

Figure 3. Histograms of the V_S and V_P/V_S retrieved after reversible-jump Markov Chain Monte Carlo inversion of surface waves data and receiver functions. The shaded areas are the uniform prior distributions for the two variables (see Table 1).

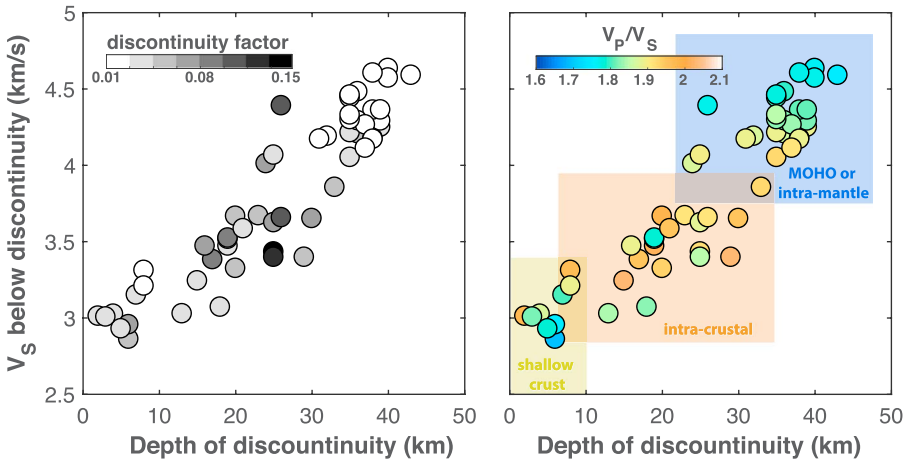

Figure 4. Ensemble solution in terms of posterior probability density function for V_S, V_P/V_S (with 1σ uncertainty) and discontinuity, as a function of depth, at station AOI on the Adriatic side of the Apennines. The velocity jump at 19 km (and associated increase in V_P/V_S) is well constrained as confirmed by the sharp increase in probability of an interface. On the contrary, the deeper jumps in velocity are more gradual and their depths show higher uncertainty, confirmed by the smearing of the discontinuity probability over a large depth interval.

homogeneity of the crust. The jump in V_S and V_P/V_S at 19 km and the narrow peak in the discontinuity probability suggests a sharp interface that is well constrained by the data. The transition to mantle velocities occurs at around 27-km depth. Here, the smeared p(discontinuity) over ~5 km suggests a transitional Moho rather than a sharp interface, a feature that we observe in the majority of the locations. Other probable discontinuities, albeit with a weak impedance contrast, occur deeper, around 35- and 45-km depth.

For the best 19 stations, we plot all the inverted values of V_P/V_S against V_S and their depth (Figure 5). Three main regions can be easily recognized, corresponding to the upper crust, middle, and lower crust, and upper mantle. To find meaningful boundaries among these regions, we use a *k-means* cluster analysis (Lloyd, 1982) with k=3 and a L_1 criterion (i.e., sum of absolute difference). The clusters' boundaries and centroids (i.e., median of the clusters) are indicated in 6 by the dashed lines and crosses. The shallow crust shows the higher variability for V_P/V_S, having values ranging from 1.68 to 1.95–2. Considering their centroids, shallow crust and mantle have similar mean values of V_P/V_S, around 1.8. Interestingly, the mean V_P/V_S for the mantle is in close agreement with the ratio of V_P and V_S at these depths given in both global models such PREM (Dziewonski & Anderson, 1981) and IASPEI91 (Kennett, 1991).

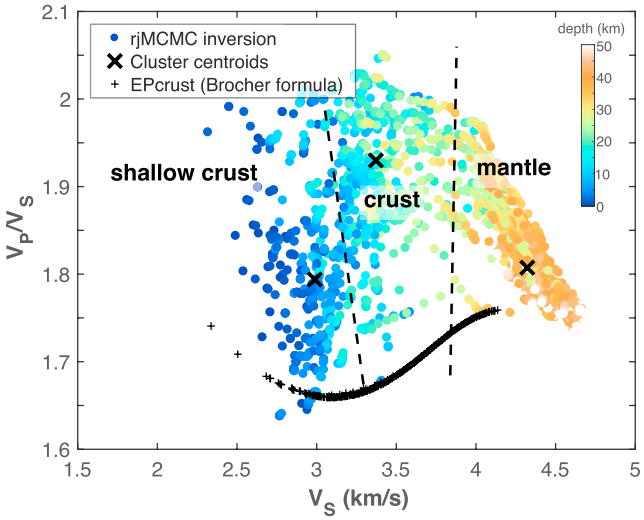

Figure 5. V_P/V_S against V_S at depth (see color scale) after inversion for all the locations. Three main regions are easily recognized, as also identified by *k-means* cluster analysis (crosses are the cluster centroids; dashed lines indicate the clusters boundaries). The shallow crust shows high variability of V_P/V_S ratio, with an average value that is comparable to that at mantle depth. The rest of the crust shows systematically higher values of V_P/V_S, in the range 1.9–2. For the sake of comparison, the V_P/V_S and V_S from EPcrust are reported: they follow the fourth-degree polynomial formula from Brocher (2005) used in EPcrust (Molinari & Morelli, 2011) to convert V_P to V_S. rj-MCMC = reversible-jump Markov Chain Monte Carlo.

The rest of the crust shows a rather distinct behavior, with remarkably higher V_P/V_S, bounded in the 1.85–2.05 range (Figure 5). Such high values are anomalous compared to expectations. For comparison, we plot the V_P/V_S and V_S as in EPcrust (Molinari & Morelli, 2011). In this model of the European crust, velocities at depth are mainly retrieved from P wave data and then converted to V_S by fourth-degree polynomial fit proposed by Brocher (2005). The poor fit between our results and those obtained using the analytic formulation of Brocher (2005) in Molinari and Morelli (2011) is indicative of the geological heterogeneity of the subsurface, which translates into complex relationships between geophysical variables (here V_P/V_S ratio and V_S). Such complexity cannot be reproduced by an empirical formula but can be imaged if complementary data sets are used, as is done in this study.

The use of RFs better constrains the depth of sharp velocity transitions. We explore the characteristics of the observed seismic discontinuities in terms of changes in V_S and V_P/V_S (Figure 6). On the left panel, we show

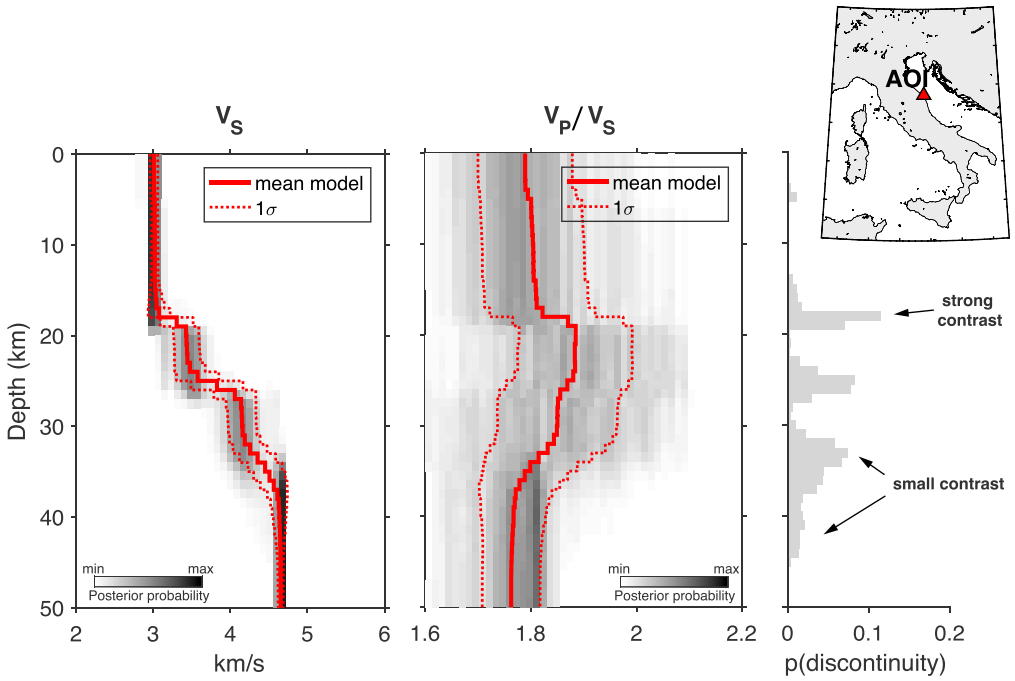

Figure 6. Left: The V_S underneath a discontinuity are reported as a function of the depth of the seismic interface for all inverted location. The "discontinuity factor" is the product of the discontinuity probability (see Figure 4, left panel) and the velocity jump in a depth interval of 2 km around the interface. Therefore, the discontinuity factor is a measure of the strength of the velocity jump and its constraint by data inversion. The discontinuities at intracrustal depths (10–30 km) are well constrained, as opposed to those of the mantle and shallow crust. In both cases the velocity jump is lower and/or its depth is more uncertain. The seismic interfaces at intracrustal depth shows also the higher V_P/V_S (see right panel). These are possibly indicative of the phase transition of quartz and used for the estimation of the geothermal gradient.

the depth of the major discontinuities and the V_S underneath. The color indicates the "discontinuity factor," a quantity that we introduce to measure the strength and uncertainty of interface in our ensemble solution. It is the product of the of p(discontinuity) and the corresponding V_S jump in a depth interval of 2 km around the interface. Thus, a gradual and/or poorly constrained interface scores a low discontinuity factor. The interfaces between 10- and 30-km depth with $V_S < 3.8$ km/s show the highest discontinuity factor, suggesting that they are strong and well constrained. Contrarily, low values of discontinuity factor are found at shallow depths, as well as at the Moho and underneath, indicating less abrupt changes in seismic velocity. In the right panel of Figure 6, the detected discontinuities are shown according to the associated variation in V_P/V_S. The velocity jumps within the crust have systematically high V_P/V_S (up to 2), whereas those detected in the mantle and the shallow crust have ratio around 1.8.

For further interpretation in terms, we select all the locations where seismic discontinuities are the strongest and well imaged at a depth of at least 10 km, having V_S smaller than 3.8 km and (iii) V_P/V_S greater than 1.8. For nine stations over 19, we find a crustal interface that satisfies these criteria. We interpret these seismic discontinuities to be caused by the transition of quartz from the α to β phase. We discuss this further in section 4.3.

4. Discussion

4.1. Data Integration: Pros and Cons

The integration of two seismological data sets has lead to important observations on both the potential and drawbacks of a joint inversion approach. At about half of our locations, the Bayesian inversion method provided a model of the subsurface that fits both the RFs and SWD data well. Considering all the stations, the normalized total misfit reveals a clear spatial pattern in the data fit (see Figure 2). For SWD data alone (Figure 2, right), at all stations our models show an overall good concordance with observed data. Stations in the Northern Apennines (NA) represent the only exception due to their relatively higher misfit, espe-

cially in the 30- to 40-s period range. At these stations, the misfit of RFs (Figure 2, left) is among the highest, suggesting that our inversion algorithm could not provide a model that fits both the RF and SWD data sufficiently well. We speculate that the reason can be found in the complex geological and tectonic setting of this area. Here, at the transition between the Apennine and Alpine orogen (Vignaroli et al., 2008), the subduction of the steep, Adriatic slab is ongoing (as attested by the compressive mechanism of seismicity), underneath the active front of the NW-SE trending fold-and-thrust belt. Our modeling of RFs is based on the assumption that seismic interfaces are flat, and this assumption might be violated in this complex environment. Anisotropy is another element that may affect both the observed Rayleigh wave phase velocities and RFs but is not accounted for in our modeling. For this area, the harmonic decomposition of the transverse component of RFs over the entire azimuthal range (Bianchi et al., 2010) revealed a NE-SW trending symmetry axis. Moreover, Plomerova et al. (2006) pointed out a complex anisotropy pattern from *SKS* splitting. Therefore, the thick and tectonized accretionary prism in the North Apenninic front may hinder the retrieval of a satisfactory model from RFs and jointly fit a complementary observable such as SWD data. Moreover, the thick sedimentary layer of the Po Plain that overlies the North Apenninic thrust represents another element of complexity. The arrivals recorded at the edge of the basin (that is the case for our stations in the NA) can be contaminated by reverberations that mask the *P*-to-*S* conversions at the Moho and intracrustal discontinuities.

If the integration of RFs and SWD has been particularly challenging in specific, geologically complex areas in the Italian peninsula, several locations are clearly on the other side of the spectrum. Our Bayesian approach performed particularly well in the Apulian platform (southeast Italy) as well as in several coastal areas in the Tyrrhenian and Adriatic sides of the Apenninic orogen. In these settings, the successful integration of the complementary data sets might be the consequence of a simpler geological setting. For example, all stations located in the Apulian platform score the lowest misfit. As a matter of fact, this area is a geologically stable, undeformed foreland consisting of a thick, horizontally layered carbonate succession from the Meso-Cenozoic (Mariotti & Doglioni, 2000). In the literature, there are no indications of seismic anisotropy that might complicate seismic wave propagation. The low-angle/horizontal layering of the carbonate succession, as well as the rather regular Moho, represent an ideal case for the RF method. It is worth noting that the Moho depth estimates obtained from our joint inversion are generally shallower (about 5km) than those obtained from the inversion of RF data only along the Apulian platform (Amato et al., 2014) and at the AOI station (Piana Agostinetti & Amato, 2009). We speculate that this difference might be attributed to different assumptions on the error statistics of the RF and SWD data. In fact, assuming a diagonal matrix for the error covariance in SWD data, while having a more realistic full covariance matrix for the RF data, means considering the SWD data more informative than RF data, implying that SWD data need to be fitted to a higher degree of precision during the rj-MCMC sampling. As discussed in Gosselin et al. (2017), a covariance matrix that is not diagonal should be more realistic for SWD errors as well.

4.2. V_P/V_S Ratio Within the Crust

For our interpretation, we focus on 19 stations where the inverted models show good agreement with both the RFs and SWD data. From our inferred velocities the crust appears rather peculiar and heterogeneous, with distinct seismic domains, likely arising from differences in lithology and mineralogical assemblages. Our results in Figure 5 are similar to those reported in Hacker et al. (2015; see Figure 6) suggesting the role of lithology and mineralogical assemblage in controlling seismic properties. Nonetheless, the strong overlap in seismic wave speeds of different rock types hinders a clear detection of lithological/mineralogical properties from seismic velocities.

The low V_P/V_S we observe in the shallow crust can be indicative of high quartz content (Birch, 1966; Christensen, 1982), a scenario that fits with an expected chemical stratification of the crust. On the other hand, the higher V_P/V_S at deeper depth can be partly explained with a decrease in quartz and increase in plagioclase content (Kern & Schenk, 1988). However, the presence of partial melts in the middle and lower portions of the crust can cause the high V_P/V_S we observe, a hypothesis that is not supported by any major decrease in V_S which would be expected for shear softening due to partial melting.

The anomalously high values we observe within the crust must involve a further mechanism. In Wang et al. (2012) numerical modeling and laboratory experiments on granite specimens suggest that high V_P/V_S (>1.9) can be reached at seismic frequencies if the rock has saturated, randomly oriented, elongated cracks. High crack density, reaching 0.2–0.25 (volume units), can explain even higher values of V_P/V_S (>2). To sustain

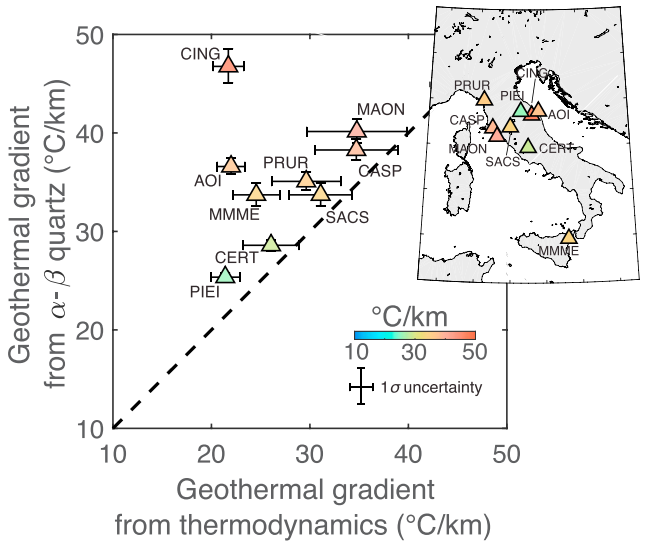

Figure 7. Geothermal gradients estimated from the *a-b* quartz transition are compared with those obtained through thermodynamic modeling (see right panel), shown on the *x* axis. Except for the stations CING and AOI, the two approaches provide similar, highly correlated values.

crack openings at middle-lower crustal depths, a high pore pressure is necessary, thus suggesting an important role of fluids within the Italian crust. Such a scenario is supported by our seismic evidence as well as by deep magnetotellurics soundings. Simpson (1999, and reference therein) reports several examples of low resistivities (10–20 Ωm) in the middle and lower crust, implying the presence of fluids in an otherwise highly resistive medium. In Italy, Patella et al. (2005) observed highly conductive bodies (<10 Ωm) below 15-km depth in the Southern Apennines. Here, both the high flux in CO_2 and the abundant mantle ^{3}He are consistent with the hypothesis of a high fluid content, possibly related to mantle sources (Italiano et al., 2000). Interestingly, Becken et al. (2008) and Ogawa et al. (2001) have observed that seismicity clusters at the transition between highly saturated geological bodies and less permeable ones, indicating a direct involvement of fluid migration for the nucleation of earthquakes. Finally, results shown in Figure 5 confirm that the use of an empirical formulation (e.g., the polynomial formula from Brocher, 2005) is unsuitable for deriving either V_S or V_P from each other when crust is complex and heterogeneous.

4.3. Temperature at Depth

Among the detected seismic discontinuities, we observe that those between 10 km and the Moho are the sharpest and best constrained by our inversion. Moreover, these are associated with high V_P/V_S ratio. Laboratory experiments on single minerals and rock aggregates (Peng & Redfern, 2013; Shen et al., 1993) and thermodynamic modeling (Diaferia & Cammarano, 2017) suggest that the $\alpha-\beta$ quartz transition is the major, seismically relevant phase change that can occur within the crust. The transition temperature is $T_q = 575$ °C at ambient pressure and varies with a gradient of 0.0256 °C/bar (e.g., $T_q = 702$ °C at 20 km and 777 °C at 30 km), according to the laboratory experiments of Shen et al. (1993). Since quartz is stiffer in its β-form, the transition is seismically marked by an increase in V_P/V_S (>1.8 in a porous-free rock aggregate, Diaferia & Cammarano, 2017) and in V_P more than in V_S. For nine locations, the strongest seismic discontinuities that we observe at crustal depth can be reasonably associated with the quartz transition. Knowing the transition temperature, we calculate the geothermal gradient at these locations, shown in Figure 7 (y axis). The width of the posterior p(discontinuity) at the discontinuity is used to evaluate the uncertainty on the gradient estimation. Since each peak of p(discontinuity) has an approximately Gaussian shape, we take the standard deviation of the best fitting Gaussian distribution to estimate the uncertainty on the depth of the interpreted quartz transition. Here the rather sharp posteriors translate into small errors in the estimation of the geothermal gradient in most of the locations ($\sigma < 1$ °C/km). Interestingly, we derive high thermal gradients, between 30 and 40 °C/km, for stations located in the Tuscan magmatic province where "orogenic" magmatism took place in the last 8.5 Ma, related to the westward subduction of the Adriatic plate and formation of the Apenninic orogen (Peccerillo & Frezzotti, 2015). The chemical signatures of both intrusive and extrusive magmatic products indicate heterogeneous mantle sources with the contamination of crustal melts and fractional crystallization within the crust. Currently, the substantial geothermal activity and the high heat flow (>100 mW/m^2; Della Vedova et al., 2001) suggest the presence of conspicuous partial melt within the crust as a residual phase of the past magmatism.

A high geothermal gradient (34 °C/km) is also observed at the station MMME, which is located 25 km NE of Mount Etna, a currently active strato-volcano in the Sicilian magmatic province. The so-called European Asthenospheric Reservoir (Lustrino & Wilson, 2007) is believed to be the deep mantle source (>400 km) causing a typical "anorogenic" magmatism (Peccerillo & Frezzotti, 2015) that is poorly affected by the nearby subduction of the Ionian slab. Such a deep source is compatible with the lower heat flow at surface (50–60 mW/m^2; Della Vedova et al., 2001) than in the Tuscan magmatic province.

At stations PIEI and CERT, we find the lowest values of geothermal gradient, 25 and 29 °C/km respectively. PIEI is located on the Apennines orogen where the high crustal thickness (35–38 km, Piana Agostinetti & Amato, 2009) is compatible with the low geothermal gradient we calculate. CERT is in the Roman magmatic province where modest and rather explosive volcanic activity occurred in the past 1 Ma, now producing diffuse CO_2 degassing. This is due to carbonate-contaminated, poorly mobile partial melts in the upper

mantle that rarely reach the shallow subsurface (Chiodini et al., 2013; Frezzotti et al., 2010), as confirmed by the moderate heat flow (Della Vedova et al., 2001).

For the stations CING and AOI we obtain very high geothermal gradients. Considering AOI as an example (Figure 4), the cause of the seismic discontinuity at 20 km is probably other than the assumed quartz transition (e.g., a strong lithological change). In fact, both AOI and the nearby CING are located on the front of the strongly tectonized, Apenninic wedge where the seismic signature of the quartz transition might be obliterated by the likely strong lithological heterogeneity occurring at depth.

The reliability of our approach based on the $\alpha - \beta$ quartz transition is tested through a comparison with an alternative method based on thermodynamics, using the absolute V_S from the model of Molinari et al. (2015). It is worth noting that this model, obtained from both phase and group velocities of Rayleigh wave, probably provides the best constraints on the absolute shear velocity. In Figure 7b, the x axis indicates the geothermal gradient obtained through thermodynamics (more details can be found in Diaferia et al., 2019). These are obtained by robust, linear fitting of lower crustal temperatures (less prone to be incorrect due to a possible underestimation of porosity) underneath each station, assuming a surface temperature of 18 °C. This allows to obtain a reasonable and representative value of geothermal gradient from seismic velocities, possibly reducing the bias associated with the specific seismic model used. In fact, as shown in Cammarano and Guerri (2017), seismic models can have rather different absolute velocities (and likewise the inferred temperatures) despite a high degree of similarity in their spatial patterns. The error on the estimate of geothermal gradient is evaluated considering the 68.3% (1σ) confidence interval of the slope of the best fitting line. Temperatures inferences through thermodynamics come with an uncertainty, however the similarity between the two independent methods is remarkable, as indicated by the vicinity of the estimated geothermal gradients to the one-to-one line. Interestingly, by using thermodynamics we find gradients at stations CING and AOI that closely resemble the value at the nearby PIEI, as one would expect. This result strengthens the hypothesis that at CING and AOI stations the $\alpha - \beta$ quartz transition method yielded an incorrect temperature estimate. In the supporting information (Figure S3), we provide a cross section that shows the crustal temperatures as estimated through the depth of the $\alpha - \beta$ quartz transition. This is given to better elucidates both the vertical and lateral variation in temperature across the Italian Peninsula.

The two methods provide highly correlated results ($r = 0.98$, if CING and AOI are excluded). However, estimates from the $\alpha - \beta$ transition are systematically higher by 3–5 °C/km compared to thermodynamics, translating in a 90–150 °C temperature difference at 30-km depth. Deciding which approach is superior in terms of reliability is challenging. The discrepancy we observe can be alternatively interpreted as an overestimation of temperature when using the $\alpha - \beta$ transition, or an underestimation by thermodynamics. If the latter is the case, this would suggest that a more mafic chemical composition than that of Rudnick and Gao (2003) would better fit the temperature values inferred from the $\alpha - \beta$ transition. We favor this possible scenario over that of an erroneous porosity correction on the observed V_S. In fact, at depths where we infer crustal temperatures, the predicted porosity is negligible (e.g., $8 \cdot 10^{-4}$% at 20 km) as well as its effect on seismic velocities. It is important to note that the two methods we use to infer temperature rely on seismic observables but are also based on different assumptions whose validity can change depending on the area. The $\alpha - \beta$ quartz transition is dominantly temperature dependent and relies on the assumption of sufficient modal quartz in the bulk rock. In Diaferia and Cammarano (2017) we demonstrated that a quartz content below <20% vol is already sufficient to produce an appreciable increase in V_P/V_S at the transition, suggesting that especially within the upper and middle crust the detection of the quartz transition might be seismically relevant. However, caution is necessary for geologically complex areas with expected structural and lithological heterogeneity that can undermine the reliability of RFs (from which V_P/V_S are derived) due to the presence of dipping interfaces and anisotropy. Concerning the use of thermodynamics, we assume a three-layer, laterally homogeneous composition for the crust, while its actual composition can be different and not spatially homogeneous. However, the assumption of a rather uniform crust (especially the lower crust, from which we fit the geothermal gradient) is reasonable for the sake of temperature inference. The appropriateness of the two approaches can be confirmed by the coherence of our temperature inferences with the expectation regarding the Italian magmatic provinces, Apennine orogen, and their known geological setting.

Either through thermodynamics or on the quartz transition, we believe that the use of seismic velocities is a viable alternative to the thermal characterization of the crust through heat flow measurements. Heat

flow is obtained through temperature measurements in geothermal and exploration boreholes during the drilling process, mostly assuming the thermal conductivity of the drilled rock (Stein, 1995). This method suffers from a series of critical issues: (i) boreholes are scarce and represent punctual information with a limited spatial representativeness; (ii) the majority of boreholes do not exceed a few hundred meter depths, where rocks might still record the seasonal and secular fluctuations of temperature above surface; (iii) mud circulation during the drilling process obliterates the geothermal profile, requiring a certain time for it to be restored. Temperature is extrapolated beyond the borehole depth applying a steady-state heat conduction equation (Chapman, 1986). This approach, commonly used in the literature, neglects other mechanisms of heat transport, such as advection, that might be relevant especially in the upper crust. As a consequence, in active areas with relevant geothermal potential (e.g., Tuscan province), the extrapolated temperature within the crust would be overestimated if heat flow and conduction equation are used. On the other hand, areas affected by fluid downwelling, favored by the local lithological and topographic setting, would result in underestimation of the geothermal gradients and temperature at depths. Other sources of uncertainty arise from the required assumptions on the heat produced by radioactive isotopes and the thermal conductivity of crustal rocks. Our method exploits the abundance of seismic data and their large coverage to assess the temperature at depth. It can be relevant in seismically active regions for defining the BDT (Rutter, 1986). Locating the depth of the BDT is vital to estimating the crustal volumes involved in a coseismic slip, allowing the evaluation of the maximum expected earthquake magnitude in a certain area (Doglioni et al., 2011). A correct assessment of the BDT is also fundamental for understanding the mechanics of crustal deformation (Kusznir & Park, 1986), especially for what concerns fold-and-thrust belts (Carminati & Siletto, 1997).

5. Limitations

We have observed that geological complexities, combined with the assumption of the used data and limitations of the inversion strategy, can substantially affect our ability to simultaneously fit both observables. For future research, it is worthwhile to assess whether accounting for seismic anisotropy and dipping interfaces can better reconcile different RFs and SWD in complex areas.

In order to recover crustal temperatures from our seismic model, we employ a number of assumptions. The quartz transition as geothermometer must be employed with caution because, though supported by laboratory experiments and thermodynamic modeling, the interpretation of a strong, intracrustal discontinuity as the quartz transition can be doubtful. It remains impossible to discern with certainty between this mineralogical transformation and changes in lithology or chemical composition. As a result, misinterpreting a lithological change as the quartz transition can lead to erroneous estimates of geothermal gradients, as we have shown at the AOI and CING stations.

Alternatively, the temperature can be calculated through thermodynamics. Our assumption consists of a three-layer, laterally homogeneous, hydrated crust may be far from being representative of the actual crust with its vertical and lateral heterogeneity. For example, the more felsic the assumed composition, the lower the temperatures that explain the observed shear wave velocities. However, we recover geothermal gradients that are in agreement with the quartz geothermometer and that are plausible at locations where the latter failed.

6. Conclusions

The thermal characterization of the Italian crust is of key importance for a better understanding of its current geological setting and evolution. However, it is challenging due to the sparsity of heat flow data, their uncertainty, and the strong underlying assumptions.

We attempted an alternative approach based on the combination of two distinct seismic data sets (RFs and SWD), jointly inverted in a Bayesian framework to retrieve the V_S and V_P/V_S at depth.

1. In specific areas, geological complexities hamper the recovery of a satisfactory subsurface model that fits both RFs and SWD data. Conversely, in stable or less tectonized areas the integration of these data has been successful.
2. The middle and lower crust exhibit high values of V_P/V_S ratio that we interpret as the evidence of pervasive fluid-filled cracks. This interpretation is supported by detection of low resistivities in deep magnetotellurics soundings both, at global and local scales.

3. Our inversion has imaged strong and well-constrained intracrustal discontinuities. These are used for the detection of the transition from α to β quartz and calculation of the local geothermal gradients. The resulting gradients are in agreement with the known geological contest and comparable to those obtained through thermodynamics.
4. Despite the different assumptions and approximations required by each of the approaches for temperature estimation, these provide comparable results. This demonstrates that the use of seismic data to obtain crustal temperature is a viable alternative to the extrapolation of heat flow measurements with a steady-state conduction equation that are affected by limited applicability, data scarcity, and high uncertainty.

Acknowledgments
N. P. A. research is funded by Austrian Science Foundation (FWF), project M2218-N29. Support for C. G. and V. L. comes from the NSF CAREER EAR-1352214 and the Packard Foundation. Data and results are available for sharing at https://figshare.com/s/15274c7657b0fb3770a8 website.

References

Amato, A., Bianchi, I., & Agostinetti, N. P. (2014). Apulian crust: Top to bottom. *Journal of Geodynamics*, *82*, 125–137. https://doi.org/10.1016/j.jog.2014.09.007

Bayes, M., & Price, M. (1763). An essay towards solving a problem in the doctrine of chances. by the late Rev. Mr. Bayes, FRS communicated by Mr. Price, in a letter to John Canton, AMFRS. *Philosophical Transactions (1683-1775)*, *53*, 370–418.

Becken, M., Ritter, O., Park, S. K., Bedrosian, P. A., Weckmann, U., & Weber, M. (2008). A deep crustal fluid channel into the San Andreas Fault system near Parkfield, California. *Geophysical Journal International*, *173*(2), 718–732. https://doi.org/10.1111/j.1365-246X.2008.03754.x

Bianchi, I., Park, J., Piana Agostinetti, N., & Levin, V. (2010). Mapping seismic anisotropy using harmonic decomposition of receiver functions: An application to Northern Apennines, Italy. *Journal of Geophysical Research*, *115*, B12317. https://doi.org/10.1029/2009JB007061

Birch, F. (1966). Compressibility; elastic constants. Handbook of physical constants. https://doi.org/10.1130/MEM97-p97

Bodin, T., & Sambridge, M. (2009). Seismic tomography with the reversible jump algorithm. *Geophysical Journal International*, *178*(3), 1411–1436. https://doi.org/10.1111/j.1365-246X.2009.04226.x

Bodin, T., Sambridge, M., Tkalcic, H., Arroucau, P., Gallagher, K., & Rawlinson, N. (2012). Transdimensional inversion of receiver functions and surface wave dispersion. *Journal of Geophysical Research*, *117*, B02301. https://doi.org/10.1029/2011JB008560

Brocher, T. M. (2005). Empirical relations between elastic wavespeeds and density in the Earth's crust. *Bulletin of the seismological Society of America*, *95*(6), 2081–2092. https://doi.org/10.1785/0120050077

Brückl, E., Bleibinhaus, F., Gosar, A., Grad, M., Guterch, A., Hrubcová, P., & Yliniemi, J. (2007). Crustal structure due to collisional and escape tectonics in the Eastern Alps region based on profiles Alp01 and Alp02 from the ALP 2002 seismic experiment. *Journal of Geophysical Research*, *112*, B06308. https://doi.org/10.1029/2006JB004687

Cammarano, F., & Guerri, M. (2017). Global thermal models of the lithosphere. *Geophysical Journal International*, *210*(1), 56–72. https://doi.org/10.1093/gji/ggx144

Carminati, E., & Siletto, G. B. (1997). The effects of brittle-plastic transitions in basement-involved foreland belts: The Central Southern Alps case (N Italy). *Tectonophysics*, *280*(1-2), 107–123. https://doi.org/10.1016/S0040-1951(97)00135-2

Castagna, J. P., Batzle, M. L., & Eastwood, R. L. (1985). Relationships between compressional-wave and shear-wave velocities in clastic silicate rocks. *Geophysics*, *50*(4), 571–581. https://doi.org/10.1190/1.1441933

Chapman, D. S. (1986). Thermal gradients in the continental crust. *Geological Society, London, Special Publications*, *24*(1), 63–70. https://doi.org/10.1144/GSL.SP.1986.024.01.07

Chiodini, G., Cardellini, C., Caliro, S., Chiarabba, C., & Frondini, F. (2013). Advective heat transport associated with regional Earth degassing in central Apennine (Italy). *Earth and Planetary Science Letters*, *373*, 65–74. https://doi.org/10.1016/j.epsl.2013.04.009

Christensen, N. I. (1982). Seismic velocities, *Handbook of physical properties of rocks* (pp. 1–228). Boca Raton: CRC.

Connolly, J. A. D. (2009). The geodynamic equation of state: What and how. *Geochemistry, Geophysics, Geosystems*, *10*, Q10014. https://doi.org/10.1029/2009GC002540

Della Vedova, B., Bellani, S., Pellis, G., & Squarci, P. (2001). Deep temperatures and surface heat flow distribution, *Anatomy of an orogen: The Apennines and adjacent Mediterranean basins* (pp. 65–76). Dordrecht: Springer. https://doi.org/10.1007/978-94-015-9829-3_7

Di Bona, M. (1998). Variance estimate in frequency-domain deconvolution for teleseismic receiver function computation. *Geophysical Journal International*, *134*(2), 634–646. https://doi.org/10.1111/j.1365-246X.1998.tb07128.x

Di Bona, M., Lucente, F. P., & Piana Agostinetti, N. (2008). Crustal structure and Moho depth profile crossing the central Apennines (Italy) along the N42 parallel. *Journal of Geophysical Research*, *113*, B12306. https://doi.org/10.1029/2008JB005625

Di Stefano, R., Kissling, E., Chiarabba, C., Amato, A., & Giardini, D. (2009). Shallow subduction beneath Italy: Three-dimensional images of the Adriatic-European-Tyrrhenian lithosphere system based on high-quality *P* wave arrival times. *Journal of Geophysical Research*, *114*, B05305. https://doi.org/10.1029/2008JB005641

Diaferia, G., & Cammarano, F. (2017). Seismic signature of the continental crust: What thermodynamics says. An example from the Italian peninsula. *Tectonics*, *36*, 3192–3208. https://doi.org/10.1002/2016TC004405

Diaferia, G., Cammarano, F., & Faccenna, C. (2019). Thermal structure of a vanishing subduction system. An example of seismically-derived crustal temperature along the Italian peninsula. *Geophysical Journal International*, *219*(1), 239–247. https://doi.org/10.1093/gji/ggz289

Diehl, T., Husen, S., Kissling, E., & Deichmann, N. (2009). High-resolution 3-D P-wave model of the Alpine crust. *Geophysical Journal International*, *179*(2), 1133–1147. 10.1111/j.1365-246X.2009.04331.x

Doglioni, C., Barba, S., Carminati, E., & Riguzzi, F. (2011). Role of the brittle-ductile transition on fault activation. *Physics of the Earth and Planetary Interiors*, *184*(3-4), 160–171. https://doi.org/10.1016/j.pepi.2010.11.005

Dziewonski, A. M., & Anderson, D. L. (1981). Preliminary reference Earth model. *Physics of the earth and planetary interiors*, *25*(4), 297–356. https://doi.org/10.1016/0031-9201(81)90046-7

Efron, B., & Tibshirani, R. (1991). Statistical data analysis in the computer age. *Science*, *253*(5018), 390–395. 10.1126/science.253.5018.390

Faccenna, C., Becker, T. W., Auer, L., Billi, A., Boschi, L., Brun, J. P., & Piromallo, C. (2014). Mantle dynamics in the Mediterranean. *Reviews of Geophysics*, *52*, 283–332. https://doi.org/10.1002/2013RG000444

Finetti, I. R. (2005). *CROP project: Deep seismic exploration of the Central Mediterranean and Italy*, Atlases of Geoscience (Vol. 1, pp. 785). Amsterdam: Elsevier.

Frezzotti, M. L., Peccerillo, A., & Panza, G. (2010). Earth's CO_2 degassing in Italy. *Journal of the Virtual Explorer*, *36*, paper 18, https://doi.org/10.3809/jvir-tex.2010.00227

Gao, C., & Lekic, V. (2018). Consequences of parametrization choices in surface wave inversion: insights from transdimensional Bayesian methods. *Geophysical Journal International*, *215*(2), 1037–1063. https://doi.org/10.1093/gji/ggy310

Gosselin, J. M., Dosso, S. E., Cassidy, J. F., Quijano, J. E., Molnar, S., & Dettmer, J. (2017). A gradient-based model parametrization using Bernstein polynomials in Bayesian inversion of surface wave dispersion. *Geophysical Journal International*, *211*(1), 528–540. https://doi.org/10.1093/gji/ggx323

Gualtieri, L., Serretti, P., & Morelli, A. (2014). Finite-difference p wave travel time seismic tomography of the crust and uppermost mantle in the Italian region. *Geochemistry, Geophysics, Geosystems*, *15*, 69–88. https://doi.org/10.1002/2013GC004988

Guerri, M., Cammarano, F., & Connolly, J. A. (2015). Effects of chemical composition, water and temperature on physical properties of continental crust. *Geochemistry, Geophysics, Geosystems*, *16*, 2431–2449. https://doi.org/10.1002/2015GC005819

Hacker, B. R., & Abers, G. A. (2004). Subduction factory 3: An Excel worksheet and macro for calculating the densities, seismic wave speeds, and H_2O contents of minerals and rocks at pressure and temperature. *Geochemistry, Geophysics, Geosystems*, *5*, Q01005. https://doi.org/10.1029/2003GC000614

Hacker, B. R., Kelemen, P. B., & Behn, M. D. (2015). Continental lower crust. *Annual Review of Earth and Planetary Sciences*, *43*, 167–205. https://doi.org/10.1146/annurev-earth-050212-124117

Haskell, N. A. (1953). The dispersion of surface waves on multilayered media. *Bulletin of the seismological Society of America*, *43*(1), 17–34.

Hastings, W. K. (1970). Monte Carlo sampling methods using Markov chains and their applications. *Biometrika*, *57*(1), 97–109. https://doi.org/10.2307/2334940

Holland, T. J. B., & Powell, R. (1998). An internally consistent thermodynamic data set for phases of petrological interest. *Journal of Metamorphic Geology*, *16*(3), 309–343. https://doi.org/10.1111/j.1525-1314.1998.00140.x

Italiano, F., Martelli, M., Martinelli, G., & Nuccio, P. M. (2000). Geochemical evidence of melt intrusions along lithospheric faults of the Southern Apennines, Italy: Geodynamic and seismogenic implications. *Journal of Geophysical Research*, *105*(B6), 13,569–13,578. https://doi.org/10.1029/2000JB900047

Kästle, E. D., El Sharkawy, A., Boschi, L., Meier, T., Rosenberg, C., Bellahsen, N., & Weidle, C. (2018). Surface wave tomography of the Alps using ambient-noise and earthquake phase velocity measurements. *Journal of Geophysical Research: Solid Earth*, *123*, 1770–1792. https://doi.org/10.1002/2017JB014698

Kennett, B. L. N. (1991). IASPEI 1991 seismological tables. *Terra Nova*, *3*(2), 122–122.

Kern, H., & Schenk, V. (1988). A model of velocity structure beneath Calabria, southern Italy, based on laboratory data. *Earth and Planetary Science Letters*, *87*(3), 325–337. https://doi.org/10.1016/0012-821X(88)90020-9

Kusznir, N. J., & Park, R. G. (1986). Continental lithosphere strength: The critical role of lower crustal deformation. *Geological Society, London, Special Publications*, *24*, 79–93. https://doi.org/10.1144/GSL.SP.1986.024.01.09

Lachenbruch, A. H. (1970). Crustal temperature and heat production: Implications of the linear heat-flow relation. *Journal of Geophysical Research*, *75*(17), 3291–3300. https://doi.org/10.1029/JB075i017p03291

Lachenbruch, A. H., & Morgan, P. (1990). Continental extension, magmatism and elevation; formal relations and rules of thumb. *Tectonophysics*, *174*(1–2), 39–62. https://doi.org/10.1016/0040-1951(90)90383-J

Licciardi, A., Agostinetti, N. P., Lebedev, S., Schaeffer, A. J., Readman, P. W., & Horan, C. (2014). Moho depth and Vp/Vs in Ireland from teleseismic receiver functions analysis. *Geophysical Journal International*, *199*(1), 561–579. https://doi.org/10.1093/gji/ggu277

Ligorria, J. P., & Ammon, C. J. (1999). Iterative deconvolution and receiver-function estimation. *Bulletin of the seismological Society of America*, *89*(5), 1395–1400.

Lloyd, S. (1982). Least squares quantization in PCM. *IEEE transactions on information theory*, *28*(2), 129–137.

Lustrino, M., & Wilson, M. (2007). The circum-Mediterranean anorogenic Cenozoic igneous province. *Earth-Science Reviews*, *81*(1), 1–65. https://doi.org/10.1016/j.earscirev.2006.09.002

Mahalanobis, P. C. (1936). On the generalized distance in statistics. National Institute of Science of India.

Malinverno, A. (2002). Parsimonious Bayesian Markov chain Monte Carlo inversion in a nonlinear geophysical problem. *Geophysical Journal International*, *151*(3), 675–688. https://doi.org/10.1046/j.1365-246X.2002.01847.x

Mariotti, G., & Doglioni, C. (2000). The dip of the foreland monocline in the Alps and Apennines. *Earth and Planetary Science Letters*, *181*(1–2), 191–202. https://doi.org/10.1016/S0012-821X(00)00192-8

Metropolis, N., Rosenbluth, A. W., Rosenbluth, M. N., Teller, A. H., & Teller, E. (1953). Equation of state calculations by fast computing machines. *The journal of chemical physics*, *21*(6), 1087–1092. https://doi.org/10.1063/1.1699114

Molinari, I., & Morelli, A. (2011). EPcrust: A reference crustal model for the European Plate. *Geophysical Journal International*, *185*(1), 352–364. https://doi.org/10.1111/j.1365-246X.2011.04940.x

Molinari, I., Verbeke, J., Boschi, L., Kissling, E., & Morelli, A. (2015). Italian and Alpine three-dimensional crustal structure imaged by ambient-noise surface-wave dispersion. *Geochemistry, Geophysics, Geosystems*, *16*, 4405–4421. https://doi.org/10.1002/2015GC006176

Ogawa, Y., Mishina, M., Goto, T., Satoh, H., Oshiman, N., Kasaya, T., & Takahashi, Y. (2001). Magnetotelluric imaging of fluids in intraplate earthquake zones, NE Japan back arc. *Geophysical Research Letters*, *28*(19), 3741–3744. https://doi.org/10.1029/2001GL013269

Ohno, I., Harada, K., & Yoshitomi, C. (2006). Temperature variation of elastic constants of quartz across the alpha-beta transition. *Physics and Chemistry of Minerals*, *33*(1), 1–9. https://doi.org/10.1007/s00269-005-0008-3

Park, J., & Levin, V. (2016a). Anisotropic shear zones revealed by backa- zimuthal harmonics of teleseismic receiver functions:. *Geophysical Journal International*, *207*, 1216–1243. https://doi.org/10.1093/gji/ggw323

Patella, D., Petrillo, Z., Siniscalchi, A., Improta, L., & Di Fiore, B. (2005). Magnetotelluric profiling along the CROP-04 section in the Southern Apennines. CROP PROJECT: Deep Seismic Exploration of the CENTRAL Mediterranean and Italy, 263–280.

Peccerillo, A., & Frezzotti, M. L. (2015). Magmatism, mantle evolution and geodynamics at the converging plate margins of Italy. *Journal of the Geological Society*, *172*(4), 407–427. https://doi.org/10.1144/jgs2014-085

Peng, Z., & Redfern, S. A. (2013). Mechanical properties of quartz at the $\alpha - \beta$ phase transition: Implications for tectonic and seismic anomalies. *Geochemistry, Geophysics, Geosystems*, *14*, 18–28. https://doi.org/10.1029/2012GC004482

Piana Agostinetti, N. (2015). The structure of the Moho in the northern Apennines: Evidence for an incipient slab tear fault? *Tectonophysics*, *655*, 88–96. https://doi.org/10.1016/j.tecto.2015.05.013

Piana Agostinetti, N., & Amato, A. (2009). Moho depth and Vp/Vs ratio in peninsular Italy from teleseismic receiver functions. *Journal of Geophysical Research*, *114*, B06303. https://doi.org/10.1029/2008JB005899

Piana Agostinetti, N., & Faccenna, C. (2018). Deep structure of Northern Apennines subduction orogen Italy as revealed by a joint interpretation of passive and active seismic data. *Geophysical Research Letters*, *45*, 4017–4024. https://doi.org/10.1029/2018GL077640

Piana Agostinetti, N., Levin, V., & Park, J. (2008). Crustal structure above a retreating trench: Receiver function study of the northern Apennines orogen. *Earth and Planetary Science Letters*, *275*(3-4), 211–220. https://doi.org/10.1016/j.epsl.2008.06.022

Piana Agostinetti, N. P., & Malinverno, A. (2010). Receiver function inversion by trans-dimensional Monte Carlo sampling. *Geophysical Journal International*, *181*(2), 858–872. https://doi.org/10.1111/j.1365-246X.2010.04530.x

Piana Agostinetti, N., & Malinverno, A. (2018). Assessing uncertainties in high-resolution, multifrequency receiver-function inversion: A comparison with borehole data. *Geophysics*, *83*(3), KS11–KS22. https://doi.org/10.1190/geo2017-0350.1

Plomerova, J., Margheriti, L., Park, J., Babuska, V., Pondrelli, S., Vecsey, L., & Salimbeni, S. (2006). Seismic anisotropy beneath the Northern Apennines (Italy): Mantle flow or lithosphere fabric? *Earth and Planetary Science Letters*, *247*(1-2), 157–170. https://doi.org/10.1016/j.epsl.2006.04.023

Ranalli, G. (2000). Rheology of the crust and its role in tectonic reactivation. *Journal of Geodynamics*, *30*(1-2), 3–15. https://doi.org/10.1016/S0264-3707(99)00024-1

Rudnick, R. L., & Gao, S. (2003). Composition of the continental crust. *Treatise on geochemistry*, *3*, 659.

Rutter, E. H. (1986). On the nomenclature of mode of failure transitions in rocks. *Tectonophysics*, *122*(3-4), 381–387. https://doi.org/10.1016/0040-1951

Schutt, D. L., Lowry, A. R., & Buehler, J. S. (2018). Moho temperature and mobility of lower crust in the western United States. *Geology*, *46*(3), 219–222. https://doi.org/10.1130/G39507.1

Serretti, P., & Morelli, A. (2011). Seismic rays and traveltime tomography of strongly heterogeneous mantle structure: Application to the Central Mediterranean. *Geophysical Journal International*, *187*(3), 1708–1724. https://doi.org/10.1111/j.1365-246X.2011.05242.x

Shen, A. H., Bassett, W. A., & Chou, I. M. (1993). The alpha-beta quartz transition at high temperatures and pressures in a diamond-anvil cell by laser interferometry. *American Mineralogist*, *78*(7-8), 694–698.

Simpson, F. (1999). Stress and seismicity in the lower continental crust: A challenge to simple ductility and implications for electrical conductivity mechanisms. *Surveys in Geophysics*, *20*(3-4), 201–227. https://doi.org/10.1023/A:1006641922180

Steckler, M. S., Agostinetti, N. P., Wilson, C. K., Roselli, P., Seeber, L., Amato, A., & Lerner-Lam, A. (2008). Crustal structure in the southern Apennines from teleseismic receiver functions. *Geology*, *36*(2), 155–158. https://doi.org/10.1130/G24065A.1

Stein, C. A. (1995). Heat flow of the Earth. *Global earth physics: A handbook of physical constants*, *1*, 144–158. https://doi.org/10.1029/RF001p0144

Thomson, W. T. (1950). Transmission of elastic waves through a stratified solid medium. *Journal of applied Physics*, *21*(2), 89–93. https://doi.org/10.1063/1.1699629

Tork Qashqai, M., Afonso, J. C., & Yang, Y. (2018). Physical state and structure of the crust beneath the western-central United States from multiobservable probabilistic inversion. *Tectonics*, *37*, 3117–3147. https://doi.org/10.1029/2017TC004914

Verbeke, J., Boschi, L., Stehly, L., Kissling, E., & Michelini, A. (2012). High-resolution Rayleigh-wave velocity maps of central Europe from a dense ambient-noise data set. *Geophysical Journal International*, *188*(3), 1173–1187. https://doi.org/10.1111/j.1365-246X.2011.05308.x

Vignaroli, G., Faccenna, C., Jolivet, L., Piromallo, C., & Rossetti, F. (2008). Subduction polarity reversal at the junction between the Western Alps and the Northern Apennines, Italy. *Tectonophysics*, *450*(1-4), 34–50. https://doi.org/10.1016/j.tecto.2007.12.012

Vitovtova, V. M., Shmonov, V. M., & Zharikov, A. V. (2014). The porosity trend and pore sizes of the rocks in the continental crust of the earth: Evidence from experimental data on permeability. Izvestiya. *Physics of the Solid Earth*, *50*(5), 593–602. https://doi.org/10.1134/S10693513

Waldhauser, F., Kissling, E., Ansorge, J., & Mueller, S. (1998). Three dimensional interface modelling with two-dimensional seismic data: the Alpine crust-mantle boundary. *Geophysical Journal International*, *135*(1), 264–278. https://doi.org/10.1046/j.1365-246X.1998.00647.x

Wang, X. Q., Schubnel, A., Fortin, J., David, E. C., Gueguen, Y., & Ge, H. K. (2012). High Vp/Vs ratio: Saturated cracks or anisotropy effects? *Geophysical Research Letters*, *39*, L11307. https://doi.org/10.1029/2012GL051742